Computers and Electronics in Agriculture 91 (2013) 106–115

Contents lists available at SciVerse ScienceDirect

Computers and Electronics in Agriculture

journal homepage: www.elsevier.com/locate/compag

Comparison of two aerial imaging platforms for identification of Huanglongbing-infected citrus trees

Francisco Garcia-Ruiz [a], Sindhuja Sankaran [b], Joe Mari Maja [b], Won Suk Lee [c], Jesper Rasmussen [a], Reza Ehsani [b,*]

[a] Department of Agriculture and Ecology, Faculty of Life Sciences, University of Copenhagen, Højbakkegaard Alle 13, DK-2630 Taastrup, Denmark
[b] Citrus Research and Education Center/IFAS, University of Florida, 700 Experiment Station Road, Lake Alfred, FL 33850, USA
[c] Department of Agricultural and Biological Engineering, University of Florida, Gainesville, FL 32611, USA

ARTICLE INFO

Article history:
Received 21 August 2012
Received in revised form 26 November 2012
Accepted 2 December 2012

Keywords:
Unmanned aerial vehicle
Citrus disease
Classification
Support vector machine

ABSTRACT

Huanglongbing (HLB) or citrus greening disease is one of the most important diseases affecting citrus orchards in Florida and other parts of the world. The first critical step for a successful control of HLB is its detection and diagnosis. Spectroscopy has proven to yield reliable results for its early detection, minimizing the time consumed for this process. This study presents a new approach of high-resolution aerial imaging for HLB detection using a low-cost, low-altitude remote sensing multi-rotor unmanned aerial vehicle (UAV). A multi-band imaging sensor was attached to a UAV that is capable of acquiring aerial images at desired resolution by adjusting the flying altitude. Moreover, the results achieved using UAV-based sensors were compared with a similar imaging system (aircraft-based sensors) with lower spatial resolution. Data comprised of six spectral bands (from 530 to 900 nm) and seven vegetation indices derived from the selected bands. Stepwise regression analysis was used to extract relevant features from UAV-based and aircraft-based spectral images. At both spatial resolutions, 710 nm reflectance and NIR-R index values were found to be significantly different between healthy and HLB-infected trees. During classification studies, accuracies in the range of 67–85% and false negatives from 7% to 32% were acquired from UAV-based data; while corresponding values were 61–74% and 28–45% with aircraft-based data. Among the tested classification algorithms, support vector machine (SVM) with kernel resulted in better performance than other methods such as SVM (linear), linear discriminant analysis and quadratic discriminant analysis. Thus, high-resolution aerial sensing has good prospect for the detection of HLB-infected trees.

1. Introduction

According to the latest commercial citrus inventory, citrus orchards in the state of Florida represent 219,000 ha (USDA, 2011a) with about $1.145 billion on-tree value (USDA, 2011b), becoming the world's second largest orange juice production area (Spreen et al., 2006). Despite these outcomes, the change in net orchard production area has been negative since 1996, with around 55,250 ha being abandoned in 2011 in Florida (USDA, 2011a). One reason for this decline is the appearance of diseases that have appeared in the last decade. One such disease is citrus greening, also known as Huanglongbing (HLB), which affects citrus production worldwide. HLB is caused by a bacterium and was first found in Florida in August of 2005, although the insect vector of this disease, psyllid (*Diaphorina citri*) was found back in 1998 (Halbert and Manjunath, 2004; Gottwald, 2010). The main symptoms that can be seen in infected trees are yellowing (chlorosis) of the leaf veins, the entire leaf or the whole branch. In case of severe infections, the disease eventually leads to the death of the tree. Fruits from HLB-infected trees grow deformed, bitter and with acidic flavor which make them unsuitable for commercial use (Chung and Brlansky, 2009). No definitive cure for this specific disease is yet known and the experts highly recommend the need for controlling the psyllid vector as a first preventive measure. In Africa, it is recommended to completely remove young infected trees, while the infected branches are removed if the trees are older than 6 years (Buitendag and von Broembsen, 1993).

The most accurate diagnosis involves polymerase chain reaction (PCR) analysis (Hansen et al., 2008) but the identification of infected trees and sampling of leaves is time consuming. Moreover, the average accuracy achieved in visually inspecting and identifying infected trees by scouts is reported to be between 47% and 59% (Futch et al., 2009). The costs of citrus greening management have raised the total citrus production costs from about 1923.15 $/ha to 4331.35 $/ha in southwest Florida from 2002–2003 to 2007–2008

* Corresponding author. Tel.: +1 863 956 8770; fax: +1 863 956 4631.
E-mail address: ehsani@ufl.edu (R. Ehsani).

0168-1699/$ - see front matter © 2012 Elsevier B.V. All rights reserved.
http://dx.doi.org/10.1016/j.compag.2012.12.002

(Muraro and Morris, 2009). Due to the severity of HLB, there is a demand for a rapid survey system to detect potentially HLB-infected trees so that the workers can focus on specified areas for monitoring, inspecting and controlling further spread of the disease.

Specific regions in the electromagnetic spectra have been found to provide information about the physiological stress in plants, and consequently, diseased plants usually exhibit different spectral signature than non-stressed healthy plants in those specific ranges (West et al., 2003; Sankaran et al., 2010). Spectroscopy in the range of visible and near infrared has been investigated for disease detection in a great variety of crops since it is a rapid and non-destructive tool that can be used in real time crop assessment under field conditions (Sankaran et al., 2010). For instance, Naidu et al. (2009) identified viral infection (leafroll) in grapevines (*Vitis vinifera* L.) under field conditions using leaf spectral response from field portable spectrometer equipped with a leaf-probe. Hyperspectral reflectance in the range of 350–2500 nm was used by Delalieux et al. (2007) to detect apple scab (*Venturia inaequalis*). The study concluded that the features along two spectral ranges in near infrared (1350–1750 nm and 2200–2500 nm) showed higher performance in the classification of infected and healthy leaves at early stages. At the same time, the spectral regions in the range 580–660 nm and 688–715 nm exhibited better classification power for developed stages of infection.

Studies on citrus diseases indicate applicability of visible-near infrared spectroscopy in remote sensing. Balasundaram et al. (2009) recommended spectral regions between 500 nm and 800 nm for successful detection of canker in citrus peel. On the other hand, HLB was detected in citrus leaves with 84–87% overall classification accuracy and an average diseased class classification accuracy of about 75–84% (Sankaran and Ehsani, 2011). In this study, quadratic discriminant analysis (QDA) and several selected bands in visible (537 nm, 662 nm, 713 nm) and near infrared (813 nm, 1120 nm, 1472 nm) performed better by themselves than introducing vegetation indices as classification features. Similar conclusion was achieved by Sankaran et al. (2011), using uncorrelated principal components computed from entire visible-near infrared spectra (350–2500 nm) as classification features. QDA distinguished between healthy and symptomatic HLB-infected leaves with accuracies greater than 90%, and 88% accuracy was found when asymptomatic leaves were included in the classification. Similarly, Mishra et al. (2011) found that low-cost optical sensor with customized spectral bands (570 nm, 670 nm, 870 nm, 970 nm) can also be used for reliable classification.

As visible and near infrared spectroscopy provides an accurate tool for plant status monitoring, it has been implemented in a wide variety of decision support systems in agriculture both in ground and aerial remote sensing. Potential applications of aerial remote sensing platforms have opened in the last few years with the availability of smaller autonomous aerial platforms capable of flying at low altitudes and diverse set of miniaturized sensors (Berni et al., 2008; Zarco-Tejada et al., 2012). Therefore, combination of Unmanned Aerial Vehicles (UAVs) with multispectral and hyperspectral cameras are becoming prevalent for weed detection and mapping for site specific herbicide application (Kazmi et al., 2011; Fernandez-Quintanilla et al., 2011), water stress detection and decision support (Sepulcre-Cantó et al., 2006; Berni et al., 2009a,b; Zarco-Tejada et al., 2012) and yield estimation (Swain et al., 2010) among others. In addition, disease detection with aerial remote sensing hyperspectral imagery is also being investigated. Zhang et al. (2005) successfully detected late blight disease in tomato fields using multispectral images at 1 m spatial resolution when the infection stage reached at least third level. Although moderate accuracies (Kumar et al., 2012) can be achieved using aerial images acquired from aircrafts, there is a need for high resolution images to further improve the identification of diseased trees. This is especially important for HLB, where symptoms may be observed only in a part of a tree (which can be at the top of the canopy), while remaining tree canopy appears healthy.

In this study, we examine the applicability of high-resolution multi-band imaging for HLB detection in citrus, while implementing a low-cost, remote sensing platform. The sensor was incorporated on an UAV that is capable of acquiring aerial images at desired resolution by adjusting the flying altitude. Our specific objectives were to: (1) to study the effect of image resolution (at two levels) on the classification performance while identifying HLB-infected trees, and (2) to identify prominent spectral features that contribute towards the healthy and HLB-infected tree classification. For the classification studies, Linear Discriminant Analysis (LDA), QDA and Support Vector Machine (SVM) were selected. The UAV images were compared with airborne multispectral images acquired from a hyperspectral camera mounted on the aircraft.

2. Materials and methods

2.1. Airborne hyperspectral images

On 14 December, 2011, airborne hyperspectral images (HYS) were acquired by Galileo Group Inc. (Melbourne, FL, USA) from a citrus orchard managed by the Citrus Research and Education Center (CREC), University of Florida, in Lake Alfred, FL using a single-engine fixed-wing aircraft. Two flight lines were carried on from 12:00 to 13:00 PM (local time), covering an area of approximately 17 ha, with coordinate center 28°07′48.30″N, 81°43′01.70″W. The flying altitude was 640 m above the sea level (around 590 m above ground level) at a speed of 65 knots. The images were taken under clear sky conditions with few scattered clouds at about 1500 m, mean solar azimuth of 182° and elevation of 38°. The camera used for this operation was an AISA EAGLE VNIR Hyperspectral Imaging Sensor (Specim Ltd., Oulu, Finland), with 397–998 nm spectral range and 128 spectral bands for the VNIR region, with spectral resolution of around 5 nm. The whole mosaic was represented by 785 × 871 pixels with a ground sampling distance (GSD) of 0.5 m and field of view (FOV) of 34°. Image data was radiometrically, atmospherically and geometrically corrected and passed a quality test by Galileo Group Inc. before being delivered. The data was atmospherically corrected using trap reference spectra. The projection used for georectification was UTM zone 17 North, WGS-84, meter. Each pixel in the image data set was delivered in reflectance × 10,000 and only the bands required for this study were converted to 8-bit format (0–255 radiometric range) with ENVI software (version 4.7, ITT VSI, White Plains, NY, USA) and stored as georeferenced raster imagery files (geoTIFF).

2.2. UAV and multiband sensors

An unmanned aerial vehicle (HiSystems GmbH, Moormerland, Germany) was used in this study (Fig. 1). It weighs about 2000 g without the camera and is powered by a 6600 mA h Lithium Ion Polymer battery which has a flight time of about 10–20 min depending on the payload. It uses six brushless motors where each motor can handle 20 A power with a maximum thrust of 2200 g. Beachwood propellers (Xoar International, CA, USA) for each motor were used to minimize the vibration in the UAV. An array of onboard sensors for flight stability and waypoint navigation includes gyroscope, accelerometer, compass, GPS, and pressure sensor. The UAV has the capability of holding its current position with up to 50 km/h wind condition. It can go up to 1 km vertically, but due to the nature of our data collection and with the Federal Aviation

Fig. 1. UAV with multiband sensor used for data acquisition from citrus orchard.

Administration (FAA) regulations, an altitude of 100 m was used. The radio transmitter (Graupner, Stuttgart, Germany) has a range of up to 4 km. Telemetric information can either be viewed on a laptop through a wireless module or directly using a radio control transmitter. Waypoints navigation can be uploaded through the laptop and can be updated while the UAV is in flight. The UAV is capable of navigation with up to a maximum of 30 waypoints using the current firmware. A small control board was added to control the trigger of the sensor attached to the UAV. This control translates the stick movements of the radio transmitter to trigger the multispectral camera.

A six narrow-band multispectral camera (miniMCA6, Tetracam, Inc., CA, USA) was attached to the UAV (Fig. 1). The camera weighs 700 g and consists of six digital image sensors arranged in a 3×2 array with independent optics and user customizable 10 nm band pass filters (Andover Corporation, NH, USA). Each of these units holds a 1.3 megapixel CMOS sensor, with image resolution of 1280×1024 pixels, 8.5 mm focal length and FOV of $43.7° \times 35.6°$. The multispectral camera was configured with two different narrow-band filter arrays. The first array was configured with filters centered at 530, 610, 690, 740, 850 and 900 nm, and the second array used filters centered at 440, 480, 560, 660, 710 and 810 nm (10 nm bandwidth). The bands were selected based on our previous work (Sankaran et al., 2011) and preliminary studies.

2.3. Data collection

A 0.35 ha plot was selected as a region of interest (ROI) from citrus orchard for this study (Fig. 2a). The orchard consisted of productive orange trees of Valencia cultivar (Swingle rootstock), grown with a row spacing of $4.6 \text{ m} \times 6.1 \text{ m}$. The plot selected as ROI for carrying on the experiments was ground scouted (visual inspection) in order to identify the trees with few symptomatic leaves to be included in the study. Two categories of trees were selected: healthy and HLB-infected trees. The GPS position of each identified tree was recorded with an RTK-GPS (HiPerXT GPS System, Topcon, Livemore, CA, USA), and a shapefile indicating the location of the healthy and HLB-infected trees was generated using ArcView GIS software (ESRI, Redlands, CA, USA). A total of 38 trees were selected, 19 healthy and 19 HLB-infected trees (Fig. 2b). Presence of HLB was confirmed through polymerase chain reaction (PCR) test in laboratory as many infected trees did not exhibit visible symptoms in their leaves.

On 14 February and 8 March, 2012, the UAV equipped with a multispectral camera was sent to a pre-defined waypoint (28.12861°, −81.71566°) within the ROI area and altitude of 100 m above the ground level for image acquisition. Once the UAV reached in assigned position and was sufficiently stable, image trigger was activated manually several times from the remote control, and about five images were captured during each flight. As the payload supported by the UAV limited the use of one camera at a time, on 14 February first camera array was used; while on 8 March second camera array was used. The camera attached directly to the UAV frame (without supplementary gimbal) and was triggered through an RS232 connection. The images were stored in 8-bit RAW format in individual compact flash cards and converted afterwards to non-compressed 8-bit TIFF format using Tetracam's software PixelWrench2 (version 1.0.6.1, Tetracam, Inc., CA, USA). Due to the low altitude at which the images were taken, solar radiation reflected by the Earth's surface to image sensors is expected to have minimal interaction with the atmosphere. For this reason, high-resolution images were not atmospherically corrected.

2.4. Ground control points and georeferencing

Eight, white $60 \text{ cm} \times 60 \text{ cm}$ boards, with a black cross in the center were used as ground control points (GCPs). They were distributed over the field, close to the corners of the area to be imaged, and their coordinates were recorded with RTK-GPS equipment. As the six-band camera yields a grayscale image per sensor per band, each of these images was georeferenced separately using the GCP coordinates. ENVI software (Exelis Visual Information Solutions, Inc., Boulder, CO, USA) was used for image registration and the images were stored as geoTIFF files. In order to match the hyperspectral image coordinates, same projection and datum was used for high-resolution images (UTM zone 17 North and WGS-84). Nearest neighborhood was selected as a resampling method.

2.5. Spectral bands and vegetation indices

Matlab (R2011a, MathWorks, MA, USA) was used for image processing and statistical analysis. The trees within the region of interest were manually segmented for both aircraft and UAV-based high-resolution georeferenced images, and a mask was generated based on the normalized difference vegetation index (NDVI) index. The trees in the image were segmented using 0.2 threshold value for NDVI such that the pixels covering the tree canopy were included in the analysis, while pixels covering the soil (non-vegetation region) were excluded. After masking, two libraries were created, one for aircraft-based and other for UAV-based images, such that there were 12 false color images (for each band) for each tree. We selected six bands out of these false color images based on our previous work and also, the need for certain bands to compute vegetation indices. Our previous work involved spectral evaluation of the 12 bands based on their separability test to detect HLB (Sankaran et al., in preparation) during ground-based remote sensing studies.

The six bands selected were 530, 560, 660, 690, 710 and 900 nm. From 128 spectral bands in the airborne hyperspectral images, bands as close to these six bands were selected. Thus, the bands from airborne images were 532, 560, 660, 688, 712 and 900 nm. Here on, a "b" preceding the wavelength value of the hyperspectral images will refer to the grayscale image captured using such filter (e.g. b900). Similarly, images from bands 532, 688 and 712 extracted aircraft-based hyperspectral data will be labeled as b530, b690 and b710 to match the labels used in the UAV-based multispectral camera.

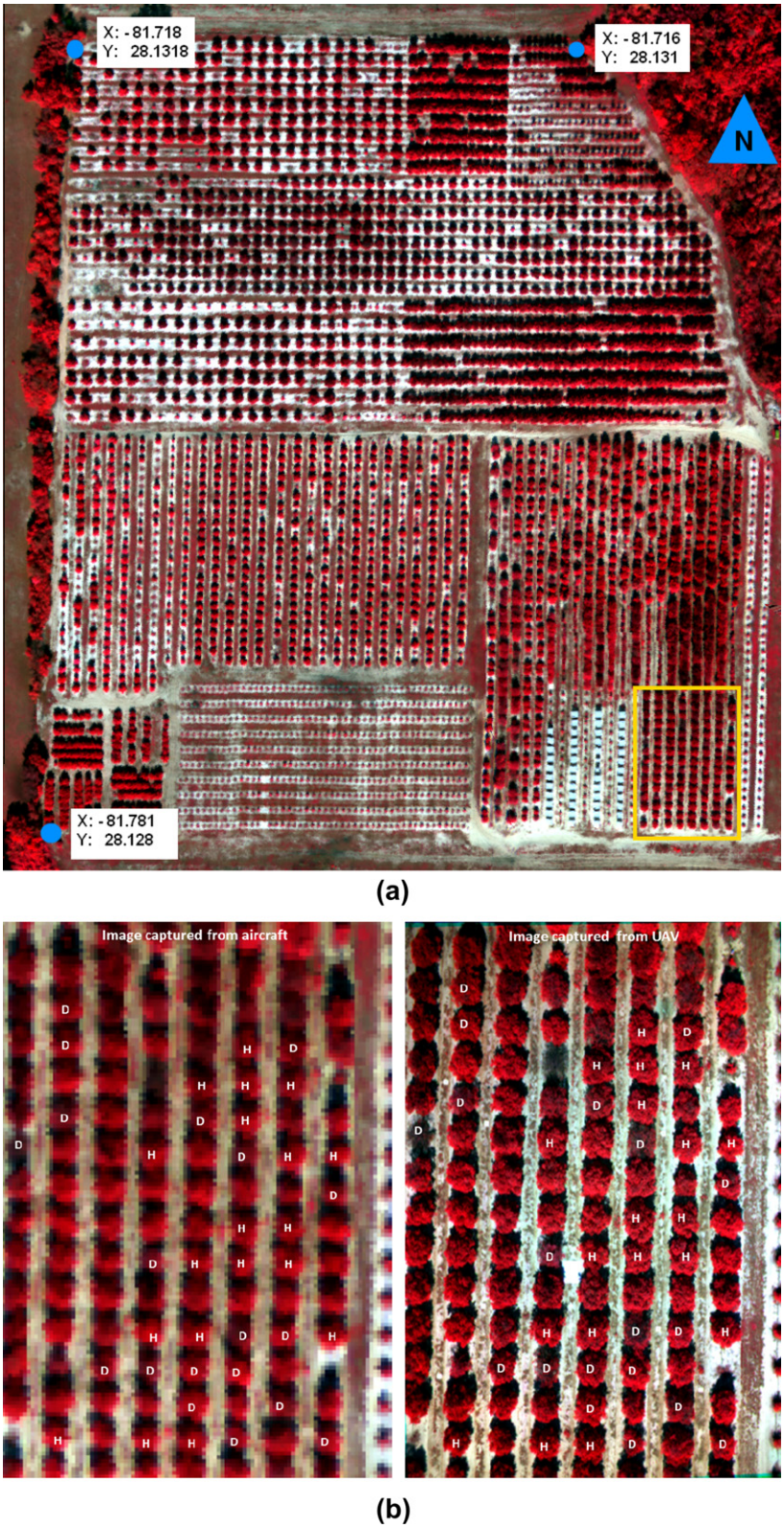

Fig. 2. (a) False color image of the study area with marked region of interest (ROI); (b) Aerial images with marked Healthy (H) and HLB-infected trees (D) within the ROI as acquired from aircraft (left) and UAV (right).

In addition to the six spectral bands, seven vegetation indices (VIs) were calculated. These indices represent plant health and photosynthetic activity. The indices studied were: NDVI, green normalized difference vegetation index (GNDVI), soil-adjusted vegetation index (SAVI), near infrared (NIR) – red(R), R/NIR, green (G)/R and NIR/R (Sankaran et al., 2010). Grayscale images representing reflectance at three spectral bands in infrared (900 nm), red (690 nm) and green (530 nm) were used for computing the

vegetation indices. Thus, the total number of spectral features was 13 per sample, which include six spectral bands and seven vegetation indices.

2.6. Feature extraction and classification

Stepwise regression analysis (Matlab) was used as a feature extraction tool in order to further reduce the number of features in aircraft- and UAV-based datasets. The function "*stepwisefit*" used begins by fitting a model without features/variables and including features one by one by comparing the *p*-value of the *F*-statistic with the entrance/exit tolerances (i.e. 0.10 and 0.15, respectively) until further improvement is sort. After feature extraction process, classification studies were conducted to assess their impact on the accuracies.

Linear and quadratic discriminant analysis as well as support vector machine (with linear and non-linear/kernel fitting), were chosen as classification algorithms. Each dataset (aircraft and UAV-based, with and without feature extraction) was divided into balanced (i.e. equal number of healthy and HLB-infected trees) calibration and validation datasets. The calibration datasets were allocated 66% of the samples and 33% for validation for testing the calibration model. Thus, 26 trees were used for calibration and 12 for validation. Raw digital values and vegetation indices were directly used as input features without any further conversion. LDA builds a linear boundary between the two groups from the calibration dataset and uses this boundary for classifying unknown samples in the validation dataset. Unlike LDA, in QDA, the covariance matrix is not assumed to be equal from class to class and a quadratic model is developed for classification. Support vector machine finds a hyperplane that generates biggest margin between the two classes. The support vectors are defined as the data points closest to the hyperplane. When kernel is applied to SVM, the separation hyperplane is no longer linear and can adopt several polynomial forms. The kernel space selected was Gaussian Radial Basis Function (rbf). The scaling factor associated to the *rbf* kernel measures the area of influence that the support vector has over the data space. This value was varied from a range of 0.5–2 in order to test its performance. Accuracy of classification as well as false negatives (i.e. infected trees classified as healthy) was computed from each classification algorithm. The final value was an average of 10 iterations, creating a new random training and testing dataset with a different seed for each iteration.

3. Results and discussion

3.1. Resolution of image data

The spatial resolution of aerial images from UAV and aircraft were compared. The multispectral data from aircraft were acquired from 590 m altitude above the ground level, which covered an area of 390 × 390 m. On the other hand, UAV-based images covered 76 × 61 m in the ground. The spatial resolution in the aircraft-based spectral images was about 0.5 m/pixel, whereas the high-resolution images extracted from the multispectral camera yielded a pixel size of about 5.45 cm/pixel (Fig. 3).

There existed a small translation between images acquired from different lenses of the multispectral camera in UAV. In other words, six images representing six spectral bands did not align perfectly though it was anticipated that the images would align correctly (with negligible misalignment) at an altitude of 100 m. This could be attributed to any of these factors, e.g., lenses placement which has an offset to each other, the time it takes for each sensor to capture and the wind condition when the UAV was hovering at that particular waypoint. The misalignment had an average offset of

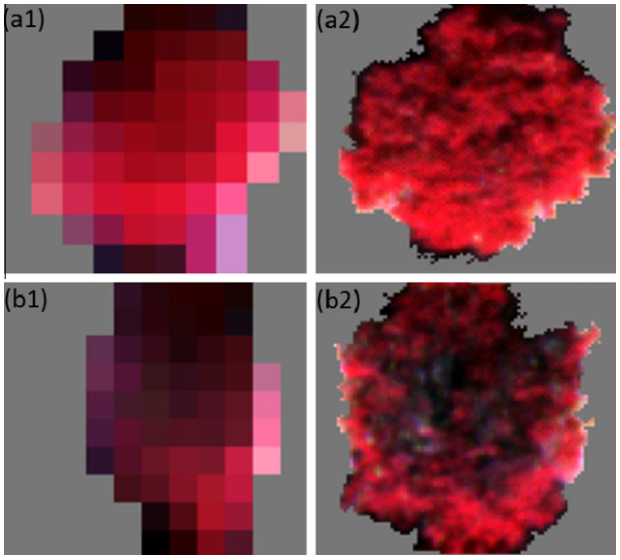

Fig. 3. False color segmented images from a healthy (a) and HLB-infected (b) tree. The images a1 and b1 represent aircraft-based images; while, images a2 and b2 represent UAV-based images. False color images were generated using *R* = 900 nm, *G* = 690 nm and *B* = 560 nm. (For interpretation of the references to color in this figure legend, the reader is referred to the web version of this article.)

eight pixels between bands. This was corrected after georeferencing each of the images by manually matching the features (control points) from one band to another and performing a projective spatial transformation. However, the multispectral images from aircraft did not display any of the above explained problems as the hyperspectral camera used is based on a single lens. The UAV-based images were radiometrically calibrated to confirm that the white board used as ground control points represented 100% reflectance with a digital number (DN) of 255.

The NDVI threshold of 0.2 used for tree segmentation was found to be optimal and canopy was successfully differentiated from soil and shadows in both healthy and infected trees (Fig. 3) without leaving excessive unwanted non-canopy pixels in the final image. This guarantees low quantity of noisy pixels in the final dataset. Several shadowed pixels in the edges of the tree were included in the final mask. The way the ground data was collected, categorizing healthy tree or infected tree instead of portions or branches of the tree, forced us to include all possible pixels (also edge mixed pixels) since the infected leaves could be anywhere within the tree canopy.

The segmented tree images taken from the aircraft composed of an average of 51 pixels whereas each tree in the UAV-based image composed of around 4849 pixels. This indicates that almost 100 times more pixels represented the same canopy area by the UAV-based camera, thus allowing more canopy details being covered by the sensing system. This difference is also important in terms of mixing at pixel level of different ground features since the higher the spatial resolution, the lower will be the influence the spectral mixing (i.e. there is a softer transition from pure vegetation to ground represented by higher amount of pixels). This allows better identification of ground features.

3.2. Spectral reflectance and vegetation indices

Healthy and infected trees presented variable reflectance pattern in the six bands and spatial resolution played a role in the pattern of the signal response (Fig. 4). HLB-infected trees reflected higher amount of light in the visible region of the electromagnetic spectrum, while their reflectance was weaker than healthy trees in the near infrared region, showing similar trend as those of ground

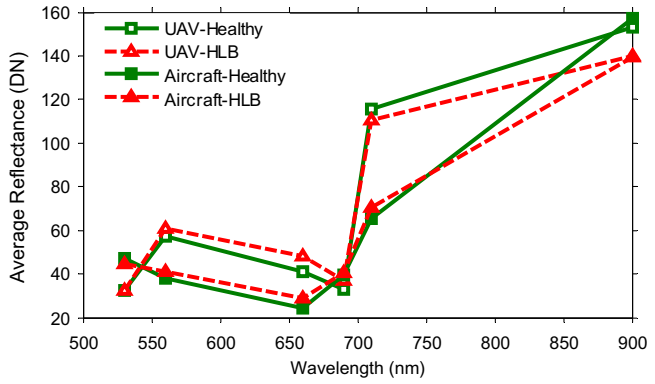

Fig. 4. Average spectral reflectance values of 19 healthy and 19 HLB-infected trees segmented from aircraft and UAV-based images.

measurements conducted by Li et al. (2012). Moreover, the UAV-based data were in agreement with the ground reflectance measurements much more often than the aircraft-based data. Statistical analysis (*t*-test with 5% level of significance) indicated that most of the DN values acquired from UAV and aircraft images were statistically different with very few exceptions. The exceptions were DN values at 690 nm for HLB-infected trees, and at 900 nm for both healthy and HLB-infected trees. The image resolution could have played a major role, which might have resulted in a lower mixing of ground features and leaf pixels in the UAV-based images.

The difference between the healthy and HLB-infected canopy reflectance was minimum at around 690 nm irrespective of spatial resolution. On the other hand, at about 710 nm, the difference due to spatial resolution of the image was maximum. Finally, at 900 nm, the reflectance values from healthy and HLB-infected trees were similar, regardless of pixel size of the image.

The indices studied reflect the plant physiological status; hence, the healthy canopy is expected to have higher values of NDVI, GNDVI, SAVI, NIR-R, G/R and NIR/R. However, plants affected by any physiological stress or perturbation (e.g. HLB bacteria) will have higher R/NIR values than healthy ones. The results showed the expected trend (Fig. 5), although differences in some indices were less prominent than in other indices. Greater differences between healthy and infected trees could be seen in indices NIR-R and NIR/R. Shadows may lead to overestimation (e.g. NDVI, SAVI, NIR/R) and underestimation (e.g. R/NIR) of some indices (Ranson and Daughtry, 1987). The shadow might have led to higher variation in NIR/R and G/R indices. There were variations in vegetation indices acquired from aircraft and UAV-based images. However, the NDVI and SAVI values were of similar range for both aircraft and UAV-based images.

3.3. Classification results

Stepwise discriminant analysis was used in order to reduce the features in the datasets leaving the ones presenting higher discriminatory power for classification. In datasets drawn from aircraft images, AC-I and AC-III, containing six and thirteen spectral features respectively, two prominent variables were found in each

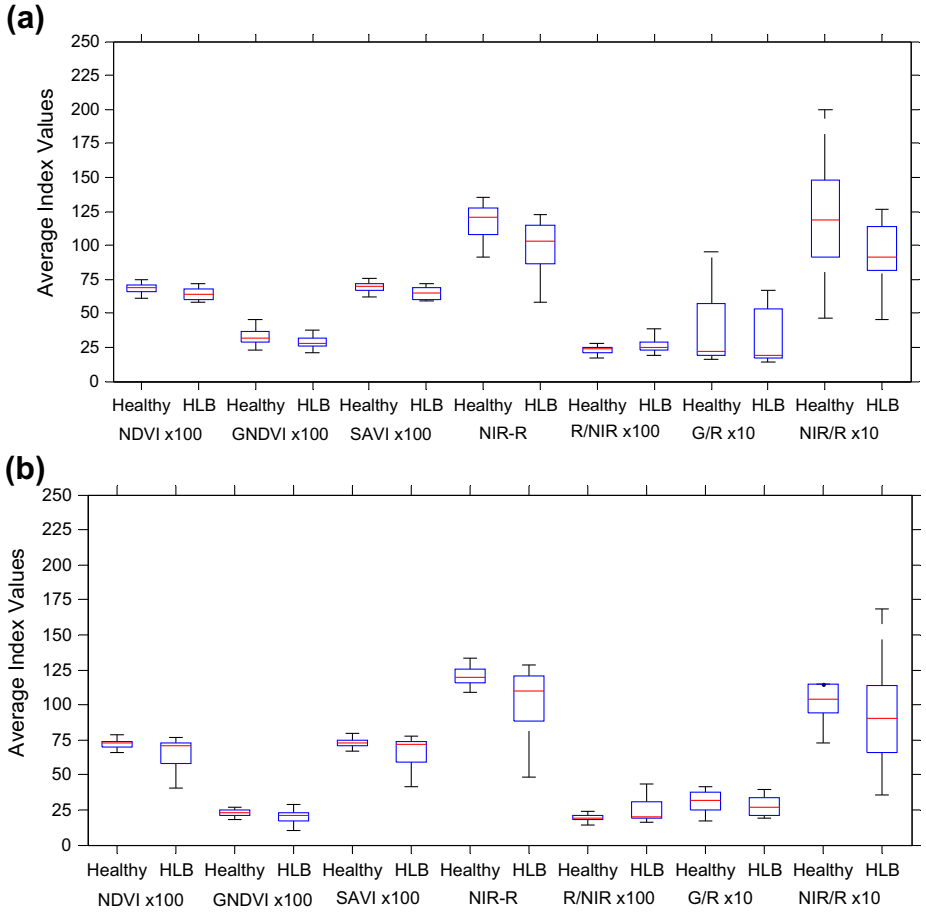

Fig. 5. Comparison of selected vegetation indices for (a) aircraft and (b) UAV-based images.

Table 1
Dataset description from aircraft (AC) and unmanned aerial vehicle (UAV)-based images. Stepwise regression analysis (sRA) used for feature reduction.

Dataset	Feature extraction method	Features
AC-I	None	b530, b560, b660, b690, b710, b900
AC-II[a]	sRA	b710, b900
AC-III	None	b530, b560, b660, b690, b710, b900, NDVI, GNDVI, SAVI, NIR-R, R/NIR, G/R, NIR/R
AC-IV[b]	sRA	b710, NIR-R
UAV-I	None	b530, b560, b660, b690, b710, b900
UAV-II[c]	sRA	b560, b710, b900
UAV-III	None	b530, b560, b660, b690, b710, b900, NDVI, GNDVI, SAVI, NIR-R, R/NIR, G/R, NIR/R
UAV-IV[d]	sRA	b560, b710, NIR-R, G/R

[a] Derived from dataset AC-I.
[b] Derived from dataset AC-III.
[c] Derived from dataset UAV-I.
[d] Derived from dataset UAV-III.

case (AC-II and AC-IV in Table 1). In the same way, datasets originated from UAV images were reduced to three (UAV-I generated UAV-II) and four variables (UAV-III generated UAV-IV). Spectral features such as b710 was common in all datasets, which indicates the significance of red-edge inflection point in vegetation spectra that indicates physiological stress (Li et al., 2012). As indicated in Table 1, AC-II and UAV-II derived from datasets AC-I and UAV-I were consistent on finding as representative features b710 and b900. In the similar fashion, AC-IV and UAV-IV derived from datasets AC-III and UAV-III, respectively found b710 and NIR-R as significant features, while in UAV-IV dataset two additional features were found (b560 and G/R) (Figs. 6 and 7).

The vegetation green peak was identified as statistically relevant only in the images taken with the UAV. This could be due to the higher spatial resolution (smaller pixel size) used in this images and narrow spectral resolution (5 nm) of the hyperspectral image acquired using aircraft. The results obtained in this study in terms of relevant representative feature selection were in accordance with previous work using ground-based spectral data (Sankaran et al., in preparation). In previous work, the reflectance values at 530, 660 and 710 nm were found to show maximum separability between healthy and HLB-infected trees.

Each of the eight datasets was randomly divided into training and testing datasets 10 times (i.e. 10 iterations). Each of the randomized datasets were reproduced such that the classification method was tested with the same dataset. The average overall classification accuracy and false negatives (i.e. infected trees classified as healthy) are summarized in Table 2. In few cases, classification accuracies could not be acquired from LDA and QDA, due to classifier limitations. The statistical analysis is also summarized in Table 3. In most cases, except QDA, there was a difference in classification accuracies and number of false negatives between aircraft and UAV-based images.

The classification using SVM algorithm (with and without kernel) resulted in higher accuracies and lower false negatives percentages (Table 2). Also the spatial resolution of the images helped to improve the classification, achieving higher performance in the datasets extracted from high-resolution UAV images (5.45 cm pixel^{-1}) than those of aircraft-based images. The highest classification accuracy was 85%, found with SVM using kernel with sigma (σ) 1.3 with high-resolution images consisting of six spectral bands (UAV-I). The lowest false negatives during classification was found with SVM classification using a dataset UAV-III composed of 13 features (six spectral bands and seven vegetation indices) where the 7% of infected trees were classified as healthy (Table 2). The best classifier would be the one that results in high classification accuracy, while maintaining low false negatives. In this study, the ideal scenario was while using UAV-I dataset and SVM with kernel (σ = 1.3) classifier that yielded 85% accuracy and 11% false negatives. SVM is a linear classifier and forms an optimal hyperplane that maximizes the margin between the classes to be separated. When a kernel is considered, the non-linear separable data is mapped to a higher dimensional space where the linear classifiers become valid. In that sense, SVM with kernel are more flexible adapting the separation plane in a more appropriate way to the data clusters. As a result, the SVM classifier with kernel allowed for a better separation and classification of the data, in comparison to other models.

In most cases, the classification accuracy improved after reducing the dataset and selecting the relevant features with stepwise regression analysis whereas there is not clear pattern concerning false negative percentage. Previous work showed that classification accuracy of about 90% could be achieved using the broad range of visible-near infrared spectra while classifying HLB-infected trees from those of healthy ones (Sankaran et al., 2011). Nevertheless,

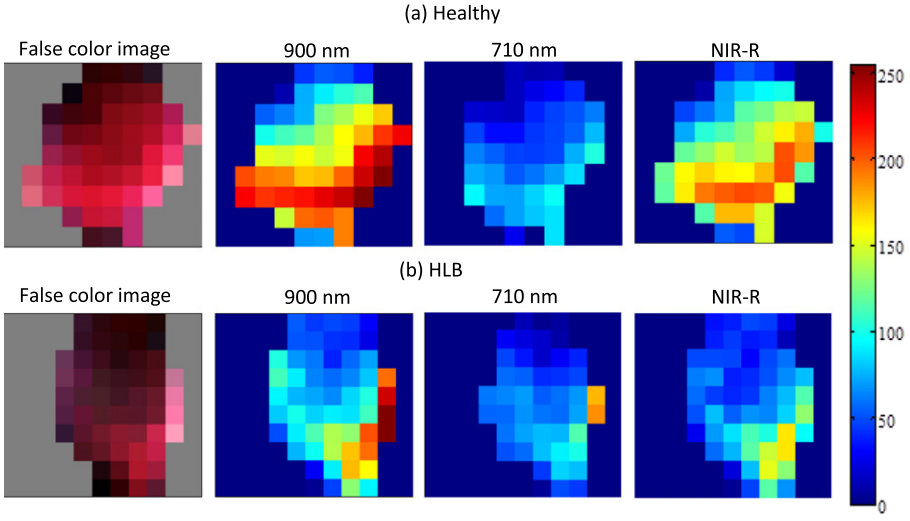

Fig. 6. False color images (R = 900 nm, G = 690 nm and B = 560 nm) and images of few significant spectral features of representative healthy and HLB-infected trees acquired from aircraft.

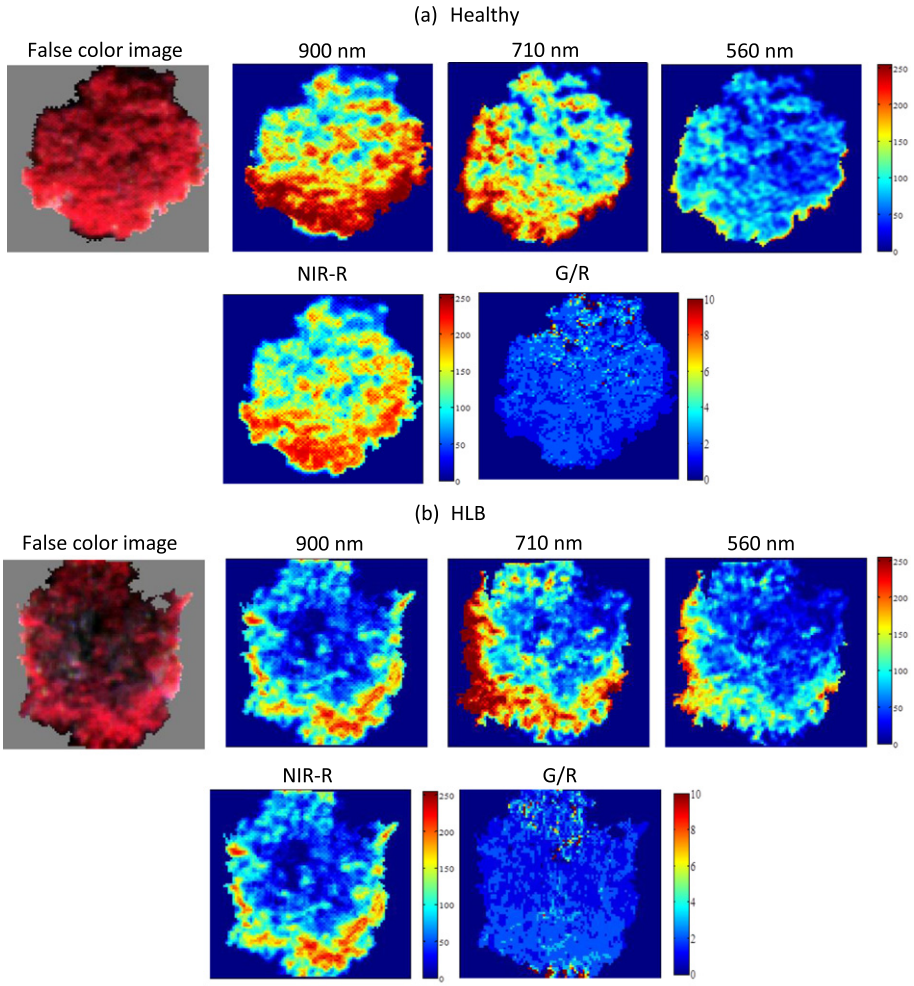

Fig. 7. False color images (R = 900 nm, G = 690 nm and B = 560 nm) and images of few significant spectral features of representative healthy and HLB-infected trees acquired from UAV-based corrected images.

Table 2
Average overall classification accuracy and false negatives (FN) after 10 iteration using linear and quadratic linear discriminant analysis (LDA and QDA) and support vector machine (SVM) without and with kernel.

Datasets	LDA		QDA		SVM		SVM (σ kernel)	
	Accuracy (%)	FN (%)	Accuracy (%)	FN (%)	Accuracy (%)	FN (%)	Accuracy (%)	FN (%)
AC-I	62	45	64	28	63	45	63 (2.0)	38
AC-II	68	37	73	40	68	40	71 (2.0)	40
AC-III	–	–	–	–	61	37	74 (2.0)	37
AC-IV	68	37	74	30	70	37	74 (2.0)	37
UAV-I	75	23	67	28	74	27	85 (1.3)	11
UAV-II	79	17	74	23	77	22	84 (0.9)	15
UAV-III	69	20	–	–	78	7	75 (1.5)	17
UAV-IV	82	32	76	23	80	20	80 (2.0)	25

Table 3
Probability values acquired from statistical analysis (t-test) comparing the aerial images acquired from aircraft and UAV, based on the classification algorithm at 5% level of significance.

Datasets	LDA		QDA		SVM		SVM (σ kernel)	
	Accuracy	FN	Accuracy	FN	Accuracy	FN	Accuracy	FN
I	0.0085	0.0046	0.6864[a]	0.1195[a]	0.0408	0.0333	0.0002	0.0022
II	0.0319	0.0006	0.8699[a]	0.2791[a]	0.0645[a]	0.0085	0.0118	0.0017
III	–	–	–	–	0.0010	0.0006	0.0007	0.0064
IV	0.0040	0.0024	0.7404[a]	0.2459[a]	0.0284	0.0177	0.1859[a]	0.1360[a]

[a] Statistically the accuracies/false negatives were not different between the aircraft and UAV-based images.

in this study, we could achieve a good classification accuracy of about 85%, which were comparable to the accuracy acquired based on similar ground-based sensors (Sankaran et al., in preparation). Pixels representing shadow region of the canopy should be avoided as recommended by Suárez et al. (2010). However, this was not carried out in this research as the area representing the infected branches was not located in the canopy, which might be in shadowed area as well. Our future studies will involve selecting the pixel of infected branches for classification to further improve the performance of the classifiers.

4. Conclusions

Multispectral images of citrus orchards were acquired at two different altitudes using multiple aerial sensing platforms, therefore, yielding different spatial resolution (0.5 m and 5.45 cm per pixel). Ground truthing of healthy and HLB-infected trees along with the GPS position was recorded and the same trees were identified and segmented from both aircraft and UAV-based images. Datasets composed of a combination of mean tree reflectance in six spectral bands and vegetation indices. Feature selection was performed using stepwise regression analysis to extract relevant features in UAV-based datasets and aircraft-based images. Features b710 nm and NIR-R index were found to be significantly different between healthy and HLB-infected trees at both spatial resolutions. However, in UAV-based images, in addition to the spectral features, b560 (green) was found to be prominent.

Four classification algorithms were used in order to classify healthy and infected trees. UAV-based datasets yielded better classification accuracy (67–85%) and lower false negatives (7–32%) than the corresponding aircraft-based datasets (61–74% and 28–45%, respectively). Among classification methods, SVM with kernel performed generally better than SVM, LDA and QDA. The best classification results with 85% accuracy and 11% false negatives were found with UAV-based aerial images, which indicate possibilities for high resolution multispectral imaging for citrus greening detection. Considering the symptoms at lower scale (i.e. branch level), images taken with UAV at low altitudes could become a reliable tool for disease detection.

Scouting is one of the key practices in HLB disease control. Aerial remote sensing with high-resolution imaging showed a great potential for detecting HLB-infected trees, and could be used as a rapid sensing technology to aid in the scouting process. This technology can reduce scouting costs and improve scouting efficiencies. Although, the sensing system in its current form is suitable for small- and medium-sized growers, the sensing platform and classification algorithm should be further improved to accommodate applications in large orchards. One of the limitations is the flight time, which depends on the payload. The UAV used in this study has a flight time of 10–20 min depending on the payload and can stay suspended in its position to acquire multiple images for a short period. Similar aerial platform could be flown for 2.5 h with 1 kg payload (Zarco-Tejada, 2011). Our future work will involve improving the image acquisition factors and study of temporal effect in aerial sensing of diseased citrus trees.

Acknowledgements

This research was a part of ongoing research efforts at Citrus Research and Education Center, Lake Alfred, FL. This research was funded by Citrus Research and Development Foundation (CRDF) and US Department of Agriculture – National Institute of Food and Agriculture (USDA-NIFA). We would like thank Ms. Sherrie Buchanon and Ms. Luba Polonik for their help during this study. Mention of company names or commercial products does not constitute endorsement or support for the use of such products.

References

Balasundaram, D., Burks, T., Bulanon, D., Schubert, T., Lee, W., 2009. Spectral reflectance characteristics of citrus canker and other peel conditions of grapefruit. Postharvest Biology and Technology 51 (2), 220–226.

Berni, J.A.J., Zarco-Tejada, P.J, Suárez, L., González-Dugo, V., Fereresa, E., 2008. Remote sensing of vegetation from uav platforms using lightweight multispectral and thermal imaging sensors. In: The International Archives of the Photogrammetry, Remote Sensing and Spatial Information Sciences, XXXVII.

Berni, J.A.J., Zarco-Tejada, P.J., Sepulcre-Cantó, G., Fereres, E., Villalobos, F., 2009a. Mapping canopy conductance and CWSI in olive orchards using high resolution thermal remote sensing imagery. Remote Sensing of Environment 113 (11), 2380–2388.

Berni, J.A.J., Zarco-Tejada, P.J., Suárez, L., Fereres, E., 2009b. Thermal and narrowband multispectral remote sensing for vegetation monitoring from an unmanned aerial vehicle. IEEE Transactions on Geoscience and Remote Sensing 47 (3), 722–738.

Buitendag, C.H., von Broembsen, L.A., 1993. Living with citrus greening in South Africa. In: Moreno, P., daGraça, J.V., Timmer, L.W. (Eds.), Proceedings of the Twelfth Conference of the International Organization of Citrus Virologists, pp. 269–273.

Chung, K.R., Brlansky, R.H., 2009. Citrus diseases exotic to Florida: Huanglongbing (citrus greening). Fact sheet PP-210. Gainesville, Fla.: University of Florida IFAS, Florida Cooperative Extension Service.

Delalieux, S., Vanaardt, J., Keulemans, W., Schrevens, E., Coppin, P., 2007. Detection of biotic stress (Venturia inaequalis) in apple trees using hyperspectral data: Non-parametric statistical approaches and physiological implications. European Journal of Agronomy 27 (1), 130–143.

Fernandez-Quintanilla, C., Dorado, J., Ribeiro, A., Gonzalez De Santos, P., 2011. RHEA: un proyecto europeo para el desarrollo de una flota de robots para el control de malas hierbas. In: Actas del XIII Congreso de la Sociedad Española de Malherbología, La Laguna, Spain, November 2011.

Futch, S., Weingarten, S., Irey, M., 2009. Determining HLB infection levels using multiple survey methods in Florida citrus. In: Proceedings Florida State Horticultural Society (FSHS), 122, pp. 152–158.

Gottwald, T.R., 2010. Current epidemiological understanding of citrus Huanglongbing. Annual Review of Phytopathology 48, 119–139.

Halbert, S.E., Manjunath, K.L., 2004. Asian citrus psyllids (Sternorrhyncha: Psyllidae) and greening disease of citrus: a Literature review and assesment of risk in Florida. Florida Entomologist 87 (3), 330–353.

Hansen, A.K., Trumble, J.T., Stouthamer, R., Paine, T.D., 2008. New Huanglongbing (Hlb) Candidatus species, "C. Liberibacter psyllaurous", found to infect tomato and potato is vectored by the psyllid Bactericerca cockerelli (Sulc). Applied and Environmental Microbiology 74 (18), 5862–5865.

Kazmi, W., Bisgaard, M., Garcia-Ruiz, F., Hansen, K.D., La Cour-Harbo, A., 2011. Adaptive Surveying and Early Treatment of Crops with a Team of Autonomous Vehicles. In: Proceedings of the 5th European Conference on Mobile Robots ECMR 2011, 7–9th September, 2011, Örebro, Sweden, pp. 1–6.

Kumar, A., Lee, W.S., Ehsani, R., Albrigo, L.G., Yang, C., 2012. Citrus greening disease detection using aerial hyperspectral and multispectral imaging techniques. Journal of Applied Remote Sensing 6, 063542. http://dx.doi.org/10.1117/1.JRS.6.063542.

Li, X., Lee, Won Suk, Li, M., Ehsani, R., Mishra, A.R., Yang, C., Mangan, R.L., 2012. Spectral difference analysis and airborne imaging classification for citrus greening infected trees. Computers and Electronics in Agriculture 83, 32–46.

Mishra, A., Karimi, D., Ehsani, R., Albrigo, L.G., 2011. Evaluation of an active optical sensor for detection of Huanglongbing (HLB) disease. Biosystems Engineering 110 (3), 302–309.

Muraro, R.P., Morris, R.A., 2009. The dynamics and implications of recent increases in citrus production costs. EDIS document FE793. Gainesville, Fla.: University of Florida IFAS, Florida Cooperative Extension Service.

Naidu, R.A., Perry, E.M., Pierce, F.J., Mekuria, T., 2009. The potential of spectral reflectance technique for the detection of Grapevine leafroll-associated virus-3 in two red-berried wine grape cultivars. Computers and Electronics in Agriculture 66 (1), 38–45.

Ranson, K., Daughtry, C., 1987. Scene Shadow Effects on Multispectral Response. IEEE Transactions on Geoscience and Remote Sensing GE-25 (4), 502–509.

Sankaran, S., Mishra, A.R., Ehsani, R., Davis, C., 2010. A review of advanced techniques for detecting plant diseases. Computers and Electronics in Agriculture 72 (1), 1–13.

Sankaran, S., Ehsani, R., 2011. Visible-near infrared spectroscopy based citrus greening detection: evaluation of spectral feature extraction techniques. Crop Protection 30 (11), 1508–1513.

Sankaran, S., Mishra, A.R., Maja, J.M., Ehsani, R., 2011. Visible-near infrared spectroscopy for detection of Huanglongbing in citrus orchards. Computers and Electronics in Agriculture 77 (2), 127–134.

Sankaran, S., Maja, J.M., Buchanon, S., Ehsani, R., in preparation. Huanglongbing (citrus greening) detection using visible-near infrared and thermal imaging techniques.

Sepulcre-Cantó, G., Zarco-Tejada, P.J., Jiménez-Muñoz, J.C., Sobrino, J.A., Miguel, E.D., Villalobos, F.J., 2006. Detection of water stress in an olive orchard with thermal remote sensing imagery. Agricultural and Forest Meteorology 136 (1–2), 31–44.

Spreen, T.H., Barber, R.E., Brown, M.G., Hodges, A.W., Malugen, J.C., Mulkey, W.D., Muraro, R.P., Norberg, R.P., Rahmani, M., Roka, F.M., Rouse, R.E., 2006. An economic assessment of the future prospects for the Florida Citrus Industry. In: Presentation to the Special Industry Task Force, Florida Department of Citrus, Lakeland, FL, March 2006. Also presented to the Board of Directors, Indian River Citrus League, Vero Beach, FL, April 2006. <http://www.fred.ifas.ufl.edu/floridajuice/pubs/EconAssessment.pdf> (accessed 23.04.12.).

Suárez, L., Zarco-Tejada, P.J., González-Dugo, V., Berni, J.A.J., Sagardoy, R., Morales, F., Fereres, E., 2010. Detecting water stress effects on fruit quality in orchards with time-series PRI airborne imagery. Remote Sensing of Environment 114 (2), 286–298.

Swain, K.C., Jayasuriya, H., Thomson, S., 2010. Adoption of an unmanned helicopter for low-altitude remote sensing to estimate yield and total biomass of a rice crop. Transactions of the ASABE 53 (1), 21–27.

USDA, 2011a. 2011 Commercial Citrus Inventory Preliminary Report. National Agricultural Statistics Service. <http://www.nass.usda.gov/Statistics_by_State/Florida/Publications/Citrus/ccipre/ccipr11.pdf> (accessed 23.04.12).

USDA, 2011b. 2010-2011 Citrus Summary Production, Price and Value Production by County and Per Tree. National Agricultural Statistics Service. <http://www.nass.usda.gov/Statistics_by_State/Florida/Publications/Citrus/cspre/cit92211.pdf> (accessed 23.04.12).

West, J.S., Bravo, C., Oberti, R., Lemaire, D., Moshou, D., Mccartney, H.A., 2003. The potential of optical canopy measurement for targeted control of field crop diseases. Annual Review of Phytopathology 41, 593–614.

Zarco-Tejada, P.J., 2011. High resolution hyperspectral and thermal remote sensing from UAV platforms for stress detection and vegetation monitoring. In: Remote Sensing Photogrammetry Society (RSPSoc) and National Center for Earth Observation (NERC) Technology Cluster UAV Workshop, 7–8th July, 2011, Durham, UK.

Zarco-Tejada, P.J., González-Dugo, V., Berni, J.A.J., 2012. Fluorescence, temperature and narrow-band indices acquired from a UAV platform for water stress detection using a micro-hyperspectral imager and a thermal camera. Remote Sensing of Environment 117, 322–337.

Zhang, M., Qin, Z., Liu, X., 2005. Remote sensed spectral imagery to detect late blight in field tomatoes. Precision Agriculture 6 (6), 489–508.